Journal of The Electrochemical Society, **157** (5) B726-B736 (2010)
0013-4651/2010/157(5)/B726/11/$28.00 © The Electrochemical Society

Effect of Cathode Pore Volume on PEM Fuel Cell Cold Start

Ashis Nandy,[a] Fangming Jiang,[a] Shanhai Ge,[a,*] Chao-Yang Wang,[a,*,z] and Ken S. Chen[b]

[a]*Electrochemical Engine Center and Department of Mechanical and Nuclear Engineering, The Pennsylvania State University, University Park, Pennsylvania 16802, USA*
[b]*Nanoscale and Reactive Processes Department, Engineering Sciences Center, Sandia National Laboratories, Albuquerque, New Mexico 87185-0836, USA*

Start-up of a proton exchange membrane (PEM) fuel cell from subzero temperatures, commonly referred to as cold start, remains a major challenge for automotive applications. In this work, we theoretically and experimentally study the effect of catalyst layer (CL) pore volume (or, more directly, CL thickness) on the cold-start performance of a PEM fuel cell for both isothermal and nonisothermal operations. Special attention is directed to determining the limits of a cold-start performance with an ultrathin CL (1 μm). The cold-start product water or the operational time approaches a minimum nonzero asymptote as the CL is gradually made infinitesimally thin. For a PEM fuel cell with standard cell thermal mass, e.g., 0.4 J/cm^2 K, and with moderately low initial membrane water content ($\lambda_0 = 7$), successful start-up from −20°C at 100 mA/cm^2 can be achieved for CL thicknesses of 10 μm and above, whereas a CL thickness of 20 μm is required for successful self-start-up from −30°C. However, successful start-up can be achieved even with a 1 μm thick CL, given certain adjustments to cell design and material properties. In particular, we study the effects of cell thermal mass and membrane water diffusivity and present a design map for self-start-up of a 1 μm CL PEM fuel cell from various subfreezing temperatures.
 [DOI: 10.1149/1.3355867]

Manuscript submitted November 24, 2009; revised manuscript received February 8, 2010. Published April 6, 2010.

Cold-start capability remains one of the greatest challenges for automotive application and commercialization of polymer electrolyte fuel cells (PEFCs). Many recent experimental and theoretical studies have been carried out to elucidate the fundamental mechanisms of cold start of a PEFC.[1-18] These studies led to the development of the intraelectrode ice formation theory,[5] which explains ice formation in the cathode catalyst layer (CCL) as the key process limiting cold-start performance and cell voltage dropdown. Fundamental research on isothermal cold start at a fixed cell temperature (below freezing) has established a basic understanding of the physics of cold start and has helped build an engineering model to evaluate the intrinsic cold-start capability of a PEFC.[3-9] More recently, based on the dependence of cold-start characteristics on cell temperature obtained from isothermal studies, many nonisothermal cold-start simulations have been performed, involving realistic automotive conditions and stack thermal environments.[13,17,19] Self-start-up from a subzero temperature depends on a delicate balance between two competing factors: heat generation with resulting temperature rise and water production or ice formation in the CCL.

Ice formation in the CCL during cold start depends on complex water flow behavior inside the cell.[3-9] As shown schematically in Fig. 1, water is produced in the CCL due to oxygen reduction reaction (ORR). Some water is transported into the CCL from the anode side due to electro-osmotic drag (EOD). Water removal from CCL occurs mainly through back-diffusion into the membrane and through vapor-phase transport from CCL into the cathode gas diffusion layer (GDL) and gas channel and finally being emitted to the ambient along with exhaust gas. The excess water increases CCL water content if initially dry, followed by water accumulation in the CCL pores in the form of ice/frost once the water vapor becomes oversaturated. For successful start-up from a subzero environment, the cell temperature should rise to the freezing point before all the pore volume in CCL is filled by frost/ice, starving the CCL of reactant gases. Thus, it is expected that the CCL pore volume, or catalyst layer (CL) thickness, is a key parameter influencing cold-start performance, as the CL pores determine the amount of ice stored before cell shutdown.

Although many studies have been performed to characterize and predict cold-start behavior under a range of operating conditions and membrane electrode properties,[20] all were focused on a standard CL with a thickness of ~10 μm, and no attention has been paid to the cold-start performance of a PEFC with a much thinner CL. As fuel cell technology moves toward a thinner CL to reduce Pt loading (such as 3M nanostructured thin-film CL with a thickness of 0.4 μm) and to remove carbon from the electrode for corrosion avoidance, understanding the cold-start consequences of these thin CLs is very important to downselect new technologies for next-generation fuel cell vehicles. In this paper, we explore the effect of CL thickness on PEFC cold start, both theoretically and experimentally. More importantly, this work aims to shed light on the desirable material and operating parameters for achieving self-start-up of a PEFC with a thin CL under automotive conditions.

The present paper is organized as follows. First, a brief description of the nonisothermal cold-start model built upon the work of Mao et al.[7] and Jiang et al.[13] is presented, with particular focus on water/heat transport and ice formation in the CCL. Next, cold-start experiments of various membrane electrode assemblies (MEAs) with different CL thicknesses are described. The Results and Discussion section then compares the predicted and measured product water as a function of the CL thickness under isothermal cold start and subsequently discusses the simulation results for both isothermal and nonisothermal cold start from −20 and −30°C over a wide range of CL thicknesses. The existence of a minimum, nonzero cold-start product water (or minimum operational time) for an infinitesimally thin CL is established. Finally, we present a design map for cell thermal mass and membrane water diffusivity, which identifies suitable material and operating parameters to achieve self-start-up of a PEFC with an ultrathin CL.

Theoretical Analysis

This section briefly describes the theoretical analysis of cold start based on a one-dimensional (1D), nonisothermal, multiphase model previously developed and used by Mao et al.[7] and Jiang et al.[13] This model can be summarized through the following governing equations[13,19]

Continuity equation

$$\frac{\partial (\varepsilon_s \rho_s)}{\partial t} + \frac{\partial (\varepsilon \rho)}{\partial t} + \nabla \cdot (\rho \mathbf{u}) = 0 \quad [1]$$

Momentum conservation

$$\frac{\partial (\rho \mathbf{u}/\varepsilon)}{\partial t} + \nabla \cdot \left(\frac{\rho \mathbf{u}\mathbf{u}}{\varepsilon^2} \right) = \nabla \cdot (\mu \nabla \mathbf{u}) - \nabla P + S_u \quad [2]$$

Species conservation

* Electrochemical Society Active Member.
z E-mail: cxw31@psu.edu

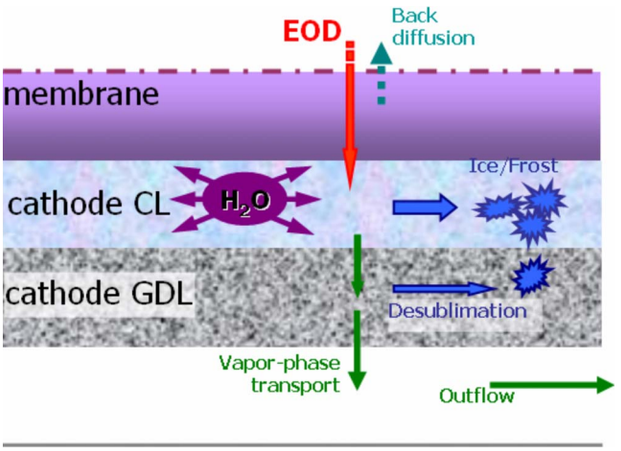

Figure 1. (Color online) Schematic diagram of water flow during cold start inside a PEFC. Redrawn after Mao and Wang.[5]

$$\frac{\partial (\varepsilon C^{\mathrm{i}})}{\partial t} + \nabla \cdot (\mathbf{u} C^{\mathrm{i}}) = \nabla \cdot (D_{\mathrm{eff}}^{\mathrm{i}} \nabla C^{\mathrm{i}}) + S_{\mathrm{C}}^{\mathrm{i}} \quad [3]$$

Charge conservation (electrons)

$$0 = \nabla \cdot (\sigma_{\mathrm{s}}^{\mathrm{eff}} \nabla \phi_{\mathrm{s}}) + S_{\phi_{\mathrm{s}}} \quad [4]$$

Charge conservation (protons)

$$0 = \nabla \cdot (\kappa_{\mathrm{e}}^{\mathrm{eff}} \nabla \phi_{\mathrm{e}}) + S_{\phi_{\mathrm{e}}} \quad [5]$$

Note that in Eq. 2, ε_{s} and ρ_{s} denote ice fraction and density of ice, respectively, which differ from ε and ρ denoting porosity and density of fluid, respectively. In this work, the multiphase model considers five sublayers of a PEFC: the anode GDL, anode CL, ionomeric membrane, cathode CL, and cathode GDL. The bipolar plates are also included in the thermal model to be discussed shortly. Convection effects are neglected in analyzing the problem of cold start.

Water transport.— Specifically, water content (λ, defined as the ratio of the number of water molecules to the number of sulfonic group, mol H_2O/mol SO_3^-) is solved for water transport in the membrane and CLs. Applying Eq. 3 to water species, a λ-explicit water transport equation in 1D form could result

$$\frac{\partial (\varepsilon_{\mathrm{eff}} \lambda)}{\partial t} = \frac{\partial}{\partial x} \cdot \left(D_{\mathrm{eff}}^{\mathrm{H_2O}} \frac{\partial \lambda}{\partial x} \right) + S_{\mathrm{C}}^{\mathrm{H_2O}} \quad [6]$$

For more details of the water diffusivity values, one can refer to Jiang et al.[13] The source term in the above equation for each subregion is given in Table I.

Water balance in cathode CL.— The importance of water flow at subzero temperatures for the fate of cold start of a PEFC is fully discussed in the previous work.[3-9,13,17] Following Mao et al.[5] and Jiang et al.,[13] water balance with respect to cathode CL is presented in Fig. 1. ORR produces water in the cathode CL at a rate of $\dot{n}_{\mathrm{pro}}$. As the visualization study of Ge and Wang[4] suggested that the freezing-point depression of water in the cathode CL is no greater than 2°C (and hence insignificant in cold-start theory), we safely assume the absence of liquid water in the cell for the entire duration of cold-start operation. Thus, water, only in the form of vapor is transported through the cathode GDL and into the gas channel and is emitted to the ambient along with the exhaust gas at $\dot{n}_{\mathrm{c,outflow}}$. Here, we assume outflow gas saturated with water vapor and negligible ice formation in the GDL due to low vapor pressure at low start-up temperatures of interest. Some water from the anode side is dragged to the cathode CL due to EOD ($\dot{n}_{\mathrm{EOD}}$). However, water diffuses into the membrane from the CCL via back-diffusion ($\dot{n}_{\mathrm{BD}}$) under the influence of a water concentration gradient across the MEA. CCL ionomers absorb water until saturation is reached, after which water starts to precipitate in the form of frost/ice in CCL pores if the local temperature remains below 0°C. The rate at which ice precipitates in the open pores of CCL is termed the ice formation rate (in mol/m^2 s). Taking the cathode CL as a control volume and denoting $\dot{n}_{\mathrm{CCL}}$ and $\dot{n}_{\mathrm{ice}}$ as the water uptake rate in the ionomers of CCL and ice formation rate in the CCL, respectively, the water balance equation is written as

$$\dot{n}_{\mathrm{pro}} + \dot{n}_{\mathrm{EOD}} + \dot{n}_{\mathrm{CCL}} + \dot{n}_{\mathrm{BD}} + \dot{n}_{\mathrm{c,outflow}} + \dot{n}_{\mathrm{ice}} = 0 \quad [7]$$

Here, $\dot{n}_{\mathrm{pro}}$ and $\dot{n}_{\mathrm{EOD}}$ are designated with a positive sign as they bring water into the cathode CL; $\dot{n}_{\mathrm{CCL}}$, $\dot{n}_{\mathrm{BD}}$, and $\dot{n}_{\mathrm{c,outflow}}$ are always designated with a negative sign as they act to take away the product water. During cold-start operation, $\dot{n}_{\mathrm{ice}}$ is considered to be negative, following the same convention described above. All the terms in Eq. 7 have a unit of mol/m^2 s.

The terms $\dot{n}_{\mathrm{pro}}$ and $\dot{n}_{\mathrm{EOD}}$ can be calculated as

$$\dot{n}_{\mathrm{pro}} = M^{\mathrm{H_2O}} \frac{I}{2F} \quad \dot{n}_{\mathrm{EOD}} = M^{\mathrm{H_2O}} \frac{n_{\mathrm{d}} I}{F} \quad [8]$$

where n_{d} denotes the EOD coefficient, which is a function of membrane water content and cell temperature.[13] Here, a uniform current distribution, I, is assumed within the CCL as the first approximation.

Water outflow along with the cathode exhaust gas can be calculated as

$$\dot{n}_{\mathrm{c,outflow}} = - M^{\mathrm{H_2O}} \xi_{\mathrm{c}} \frac{I}{4F} \frac{1}{0.21} \frac{p_{\mathrm{sat}}^{\mathrm{H_2O}}(T)}{p_{\mathrm{c}}} \quad [9]$$

The water back-diffusion rate can be calculated from the water flux at the membrane/CCL interface, such that

Table I. Source terms for the conservation equations (reproduced after Jiang et al.[13]).

	S_{u}	$S_{\mathrm{C}}^{\mathrm{H_2O}}$	S_{C} (reactants)	$S_{\phi_{\mathrm{s}}}$	$S_{\phi_{\mathrm{e}}}$
GDLs	$-\frac{\mu}{K_{\mathrm{GDL}}} u$	$-\dot{q}_{\mathrm{gs}}^{\mathrm{H_2O}}$	0	0	—
CLs	$-\frac{\mu}{K_{\mathrm{CL}}} u$	$-\nabla \left(\frac{n_{\mathrm{d}}}{F} i_{\mathrm{e}} \right) - \frac{s_{\mathrm{k}} j}{nF} - \dot{q}_{\mathrm{gs}}^{\mathrm{H_2O}}$	$-\frac{s_{\mathrm{k}} j}{nF}$	$-j$	j
Membrane	—	$-\nabla \left(\frac{n_{\mathrm{d}}}{F} i_{\mathrm{e}} \right)$	0	—	0

Note: Electrochemical reaction $\Sigma s_{\mathrm{k}} M_{\mathrm{k}}^{z} = n e^{-}$, where $M_{\mathrm{k}} \equiv$ chemical formula of species k, $s_{\mathrm{k}} \equiv$ stoichiometry coefficient, and $n \equiv$ number of electrons transferred. In PEFC anode: H_2–$2H^+ = 2e^-$; in cathode: $2H_2O$–O_2–$4H^+ = 4e^-$.

$$\dot{n}_{BD} = -M^{H_2O} D_{eff}^{H_2O} \left.\frac{\partial \lambda}{\partial x}\right|_{CCL/mem\ interface} \quad [10]$$

The water uptake rate in the ionomers of cathode CL can be determined mathematically by

$$\dot{n}_{CCL} = -\frac{M^{H_2O}}{A}\frac{\frac{\rho \varepsilon_{mem}}{EW}\int_{V,CCL}(\lambda|_{t+\Delta t} - \lambda|_t)dV}{\Delta t} \quad [11]$$

where $\lambda\,|_t$ and $\lambda\,|_{t+\Delta t}$ denote local water content in the cathode CL at two time instants, t and $t + \Delta t$, respectively. Once the ionomers in the cathode CL are water saturated, excess water remaining in the cathode CL precipitates into ice and the resulting ice fraction can be calculated as

$$s_{ice} = s_{ice,0} + \int_{t_0}^{t} \frac{(\dot{n}_{pro} + \dot{n}_{EOD} + \dot{n}_{BD} + \dot{n}_{c,outflow})\upsilon_{ice}}{M^{H_2O}\varepsilon_{CCL}\delta_{CL}}dt \quad [12]$$

where $s_{ice,0}$ denotes the initial ice fraction in the cathode CL, υ_{ice} is the molar volume of ice, and the time instant t_0 at which the water content in the cathode CL reaches the saturated value of 14 can be calculated by

$$\int_0^{t_0} \dot{n}_{CCL}dt = \frac{M^{H_2O}}{A}\frac{\rho \varepsilon_{mem}}{EW}\int_{V,CCL}(\lambda_{sat} - \lambda_0)dV \quad [13]$$

where λ_0 is the initial water content in the cathode CL.

Heat balance.— Spatially uniform cell temperature is well justified for the problem of cold start, and hence a lumped thermal model is used in the present study. The heat equation is further coupled to other conservation equations with the assumption of instantaneous ice formation. Integrating all local heat sources, the total heat generation rate during cold start is given by[17,19]

$$\dot{Q}_{total} = \frac{1}{A}\int_{V,CLs}\left[j\left(\eta + T\frac{dU_0}{dT}\right) + \frac{i_e^2}{\kappa_e^{eff}} + \frac{i_s^2}{\sigma_s^{eff}} + \dot{q}_{gs}^{H_2O}h_{gs}\right]dV + \frac{1}{A}\int_{V,mem}\frac{i_e^2}{\kappa_e}dV \quad [14]$$

Heat losses from the cell could be expressed as[17,19]

$$\dot{Q}_{loss} = \frac{1}{A}[(\dot{m}C_p)_{out}T - (\dot{m}C_p)_{in}T_0] + h(T - T_0) \quad [15]$$

The first and second terms in the right side of Eq. 15 represent heat carried away by exhaust gases and convective heat loss from bipolar plates, respectively. Under the assumption of spatially uniform cell temperature, a total energy balance to the cell can be performed to calculate the cell temperature rise as[17,19]

$$(mC_p)_{cell}(T - T_0) = \int_0^t (\dot{Q}_{total} - \dot{Q}_{loss})dt \quad [16]$$

The governing equations are discretized using a finite volume method, and the resulting algebraic equations are solved together with appropriate boundary/initial conditions in a Fortran code. Ten numerical elements were sufficient to resolve through-plane variations in the membrane, and studies of both grid-step and time-step independence were performed. All the following simulations are 1D in the through-plane direction and do not account for the variations in the in-plane or along the channel direction.

Experimental

A set of catalyst-coated membranes (CCM) was made by spray-depositing catalyst ink onto Nafion 212 membrane using a coating machine. The catalyst ink was composed of Pt/C (40 wt % Pt on Vulcan XC-72, E-TEK), water, isopropyl alcohol, and Nafion solution. The weight ratio of Nafion to the total Pt/C was 23.6:76.4. The Pt loading in the anode catalyst layer (ACL) was constant at 0.4 mg/cm^2, while that in the CCL varied between 0.1 and 0.8 mg/cm^2, yielding CL thicknesses of 2.5, 5, 10, 15, and 20 μm. The active area of all electrodes was 5 cm^2. Each CCM was sandwiched between two poly(tetrafluoroethylene)-proofed carbon papers with a microporous layer (Toray TGP-H-060) as the anode and cathode GDLs. The flow field plates for testing the MEA were made of graphite and were clamped between stainless steel plates.

The experiment procedure was the same as that reported previously.[9] In brief, both sides of the cell were purged with dry nitrogen at 55°C for 2 min. The flow rates of the anode and cathode purging gases were 400 and 900 mL/min [standard temperature and pressure (STP)], respectively. When starting up the cell at −20°C, dry hydrogen and air were fed to the cell at stoichiometric ratios of 14.35 and 12.06 (H_2 flow rate: 50 mL/min, STP; air flow rate: 100 mL/min, STP at $i = 0.1$ A/cm^2), respectively. The current density was kept constant at 0.1 A/cm^2 during each start-up, and the cell potential was recorded. Each experiment was terminated when the cell potential dropped to 0.1 V. The cold-start product water was calculated based on the measurement of the cold-start operational time and applied current density (as given by Eq. 18) and is used for model validation later.

Results and Discussion

The current model is a 1D version of the cold-start model of Mao et al.[5] and Jiang et al.[13] The present work aims to understand average cold-start behaviors of a PEFC, especially with a thin CL, and thus it suffices to consider a simple 1D model along the through-plane direction. In addition, the 1D cold-start model of Mao et al. has been extensively validated against the experimental data of product water and voltage curves over a wide range of initial and operating conditions under isothermal cold start.[7] The validation work accounted for different cold-start conditions (varying purge practice, start-up current density, and cell temperature) and different MEA designs (varying membrane thickness). The range of experimental data for the validation work is given by Tajiri et al.[8] Varying purge practice includes equilibrium purge and dry purge as explained by Tajiri et al.[8] Start-up current densities of 40 and 100 mA/cm^2 and many start-up temperatures ranging from −3 to −30°C were used for these experiments. Two different MEAs having 30 and 60 μm thick membranes were used. The predicted voltage curve and the product water agreed with the experiments. Thus, the validity of the basic physics and governing mechanisms of the PEFC cold start in this model is reasonably established. Herein, we further validate the cold-start model against experimental data for a range of CL thicknesses, as presented later in this section.

The goals of the present work are (*i*) to explore the effect of the CL thickness on PEFC cold start with special attention toward the physics of cold start with a thin CL and (*ii*) to provide a design guideline for cell design and material properties for achieving successful self-start-up of the PEFC with a thin CL (1 μm in this work) from subfreezing temperatures.

Isothermal cold start.— A set of simulations was performed to delineate CL thickness effect on isothermal cold start of a PEFC as it signifies the intrinsic water storage and cold-start capability of a PEFC. If not specified otherwise, the geometric parameters, operating conditions, and material properties used are presented in Table II. A 30 μm thick membrane is used for all simulations in this section. The electrochemical, physical, and transport properties are the same as in Jiang et al.[13] Before cold start, the cell is assumed to be prepared with equilibrium purge. In equilibrium purge, the purge gas having a controlled relative humidity is applied for several hours as described by Tajiri et al.[8] Thus, no initial ice exists in the cell before cold-start operation and the water content in the MEA becomes uniform and corresponds to the relative humidity of the purge gas. In the current study, we assume equilibrium purge with purge gas having 80% relative humidity, which translates to a water content value of 7 (representing a reasonable value for a moderately dry

Table II. Geometrical parameters, operating conditions, and material properties.

Quantity	Value
Membrane thickness	30 μm
Anode/cathode CL thickness[a]	10/10 μm
Anode/cathode GDL thickness	300/300 μm
Thermal mass of the cell, $(mC_p)_{cell}$	0.4 J/cm^2 K
Anode/cathode pressure	1.0 atm
Heat convection coefficient, h	10 W/m^2 K
Ambient start-up temperature[a]	−20°C
Current density	100 mA/cm^2
Anode/cathode stoichiometry	2.0
Anode/cathode inlet gas temperature	Same as ambient temperature
Relative humidity of anode/cathode inlet gas	0.0%
Porosity of GDL	0.6
Porosity of CL	0.5
Volume fraction of ionomer in CL	0.2
Equivalent weight of ionomers	1.1 kg/mol
Density of dry membrane	1980 kg/m^3
Initial water content in MEA, λ_i	7.0
Initial ice fraction in CL	0

[a] Baseline parameter.

MEA) according to Springer's water uptake curve.[21] The current density used throughout this study is 100 mA/cm^2.

Before discussing the effect of varying CL thickness on isothermal cold start, let us first examine the base-case result shown in Fig. 2, where the startup temperature is −20°C and the CL thickness is 10 μm. As shown in Fig. 2a, the PEFC for this base case can operate for about 76 s before cell voltage drops rapidly. The corresponding ice fraction plot shows the start of ice formation in CCL at about 16 s followed by a steady rise and, finally, ice fraction in the CCL reaching unity at about 76 s (thereby plugging all CCL pores with ice and starving the reaction sites of reactant gases, causing a cell shutdown). Water transport inside the cell plays a pivotal role in cold-start behavior; the average water content inside various components of the MEA as evolving with time is presented in Fig. 2b. CCL water content increases from 7 to the saturated value of 14 in 16 s, and thereafter, ice formation starts in the CCL (as shown in Fig. 2a). Water content of the ACL shows a gradual decrease to about 4.5 due to the dominance of EOD over the back-diffusion of water in the earlier stage of cold start, and then a small rise follows. The average membrane water content increases rather quickly in the earlier stage, but the increase gradually becomes slower, as the driving force or the gradient between the CCL and the membrane water content diminishes with time. The rise in cell voltage in the initial period is a result of reduced ohmic loss owing to the increase in membrane proton conductivity with increasing membrane water content, as given in the following relation[13]

$$\kappa_e = \exp\left[2222\left(\frac{1}{303} - \frac{1}{T}\right)\right](0.005139\lambda - 0.00326) \quad (\Omega \text{ cm})^{-1} \qquad [17]$$

The effect of CL thickness on the isothermal cold-start performance of a PEFC is shown for two ambient temperatures (−20 and −30°C) in Fig. 3. The CL thickness is varied from 20 to 0.01 μm. Such a small value of the CL thickness is chosen mainly for the fundamental understanding of the governing physics of cold-start behavior of the PEFC with a thin CL. The initial membrane water content of 7 and zero initial ice fraction in CCL are assumed in these studies. The x-axis represents the CL thickness in micrometers, whereas the y-axis of this plot gives the cold-start product water

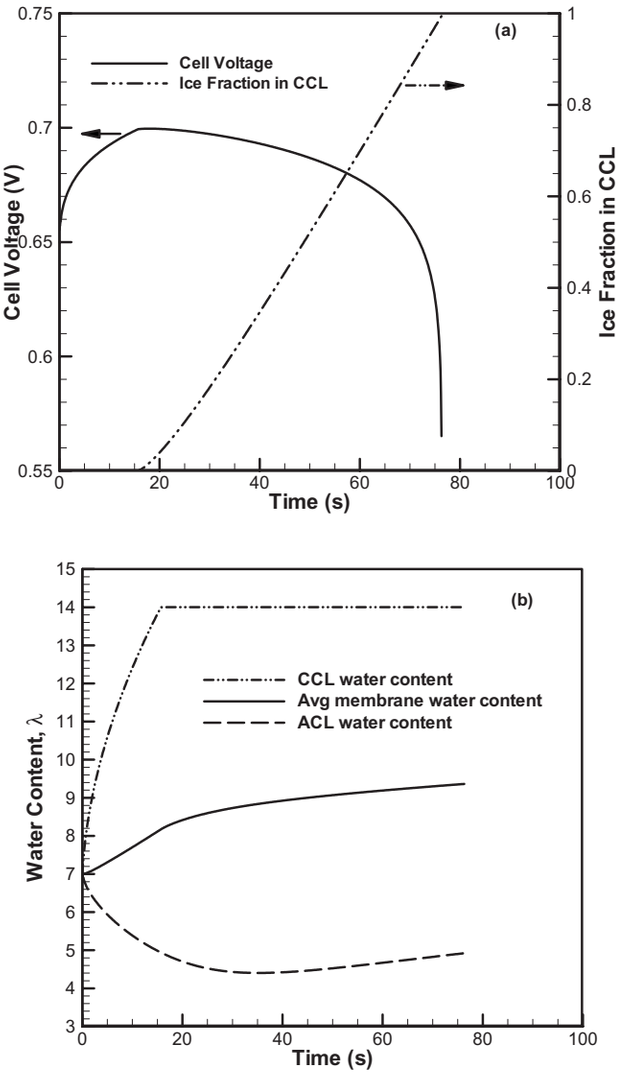

Figure 2. Baseline case result for isothermal cold-start simulation with initial membrane water content of 7 and start-up temperature of −20°C (I = 100 mA/cm^2). (a) Cell voltage and ice fraction in CCL vs time and (b) CCL, membrane, and ACL water content vs time.

before cell shutdown, which is indicative of the intrinsic PEFC cold-start capability.[7] This cold-start product water can be found from the operational time (t) as follows

$$\text{Cold start product water} = \frac{M^{H_2O} I t}{2F} \qquad [18]$$

where I is the applied current density (here, 100 mA/cm^2). As can be seen in Fig. 3, the cold-start product water decreases rather rapidly with a thinner CL (from 20 to 1 μm), but further reduction in CL thickness has little effect on the cold-start product water. The trend is true for both −20 and −30°C cases, although the cold-start product water decreases with decreasing cell temperature as expected. To explore this interesting trend, isothermal simulations are performed with a CL as thin as 0.01 μm. The product water asymptotically reaches a minimum nonzero value as the CL thickness is gradually decreased to be infinitesimally thin. This signifies that the operational time (t in Eq. 18) is not directly proportional to the CL thickness and shows a nonzero asymptotic behavior as the CL thickness approaches zero value (although intuitively one expects the

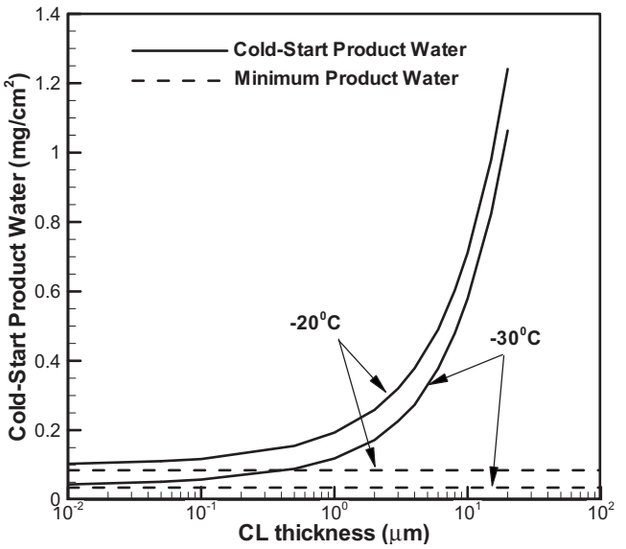

Figure 3. Cold-start product water for different CL thicknesses along with minimum theoretical product water for two different start-up temperatures (−20 and −30°C). Initial membrane water content is 7.

operational time to be proportional to the CL thickness or the CL pore volume).

To further understand the asymptotic nature of the product water (or operational time, t), the CCL water content evolution with time is shown in Fig. 4 for three different CL thicknesses (10, 1, and 0.1 μm). Let us divide the total operational time, t, in two parts: (*i*) t_1, representing the time taken by the CCL to reach λ = 14 (saturation value) or the onset of ice formation in CCL, and (*ii*) t_2, representing the ice formation time (when λ remains constant at 14). As can be seen clearly in Fig. 4, although t_2 is almost proportional to the CL thickness (as expected because the CL thickness represents the pore volume available for ice/frost precipitation), t_1 shows an asymptotic behavior, the difference between 1 and 0.1 μm cases being very small. This can be seen more clearly in the inset figure, which is zoomed in the initial period of cold start. Thus, we can

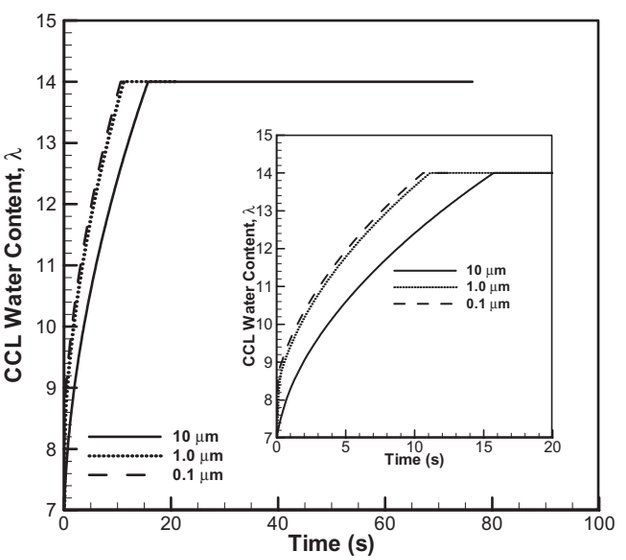

Figure 4. Water content evolution in CCL with time for three different CL thicknesses. Initial membrane water content is 7, and start-up temperature is −20°C. The same figure is zoomed and shown in the inset for 0–20 s.

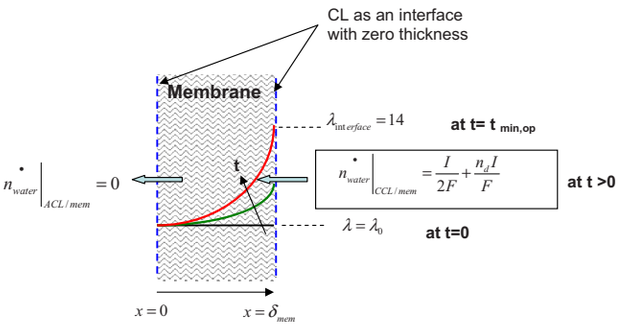

Figure 5. (Color online) Schematic illustration of water transport mechanism during cold start with infinitesimally thin CL. Note here that $t_{min,op}$ represents the end of cold-start process.

attribute the minimum cold-start product water observed in Fig. 3 to the finite time offered by water uptake into a partially hydrated membrane, regardless of the CL thickness.

The physics of the limiting case of cold start with zero CL thickness can be visualized using a model problem sketched in Fig. 5, where a membrane is coated with two catalyst interfaces without thickness. If the membrane is initially below full hydration (i.e., the initial water content is below 14 in this study), the cold-start operation can be sustained for some time and the product water is simply absorbed into the initially partially hydrated membrane. Only when the membrane water content at the interface with CCL reaches the saturation value does ice start to precipitate on the membrane surface, which immediately shuts down the zero-thickness CL. Thus, the minimum product water in this scenario corresponds theoretically to the period of membrane water absorption. By solving the water transport equation through the membrane with the appropriate boundary conditions shown in Fig. 5 and with an initial condition of water content $\lambda_0 = 7$, one can obtain the local profiles of water content shown in Fig. 6a for the cell temperature of −20°C. Figure 6b further shows the temporal evolutions of the average water content in the membrane and that at the cathode interface of the membrane. As can be seen, the cell operational time is about 9 s in this limiting case, which is very close to the operational time of the PEFC with a thin CL (compared with the 0.1 μm CL case, as shown in Fig. 4). The limiting case calculation for 30°C also shows excellent agreement with the asymptotic behavior shown in Fig. 3 (although local membrane water content evolution for this limiting case is not shown here).

The above-mentioned model MEA, consisting of a membrane coated with two catalyst interfaces without thickness, could provide an elegant experimental means to measure transport properties of the membrane under subzero temperatures, such as EOD coefficient and water diffusivity. This is because the measurable shutdown time corresponds to the onset of ice formation on the membrane surface, which in turn depends solely on the membrane transport properties.

Experimental validation.— The current analysis of CL thickness effect is validated against isothermal experiments carried out at −20°C for a set of MEAs based on Nafion 212 membrane and with a CL thickness ranging from 2.5 to 20 μm. The variable used for model validation is the cold-start product water based on the measured operational time before cell shutdown (using Eq. 18). The initial condition of the cell before cold-start operation is estimated as follows.

After gas purge, the cell is sealed and cooled down immediately, at which point the cell high frequency resistance (HFR) was measured to be 235 mΩ cm^2. However, after some time, the membrane HFR underwent relaxation, and the HFR dropped to ~150 mΩ cm^2, consistent with the relaxation curve of Tajiri et al.[22] Correcting this final cell HFR by the contact/electronic resis-

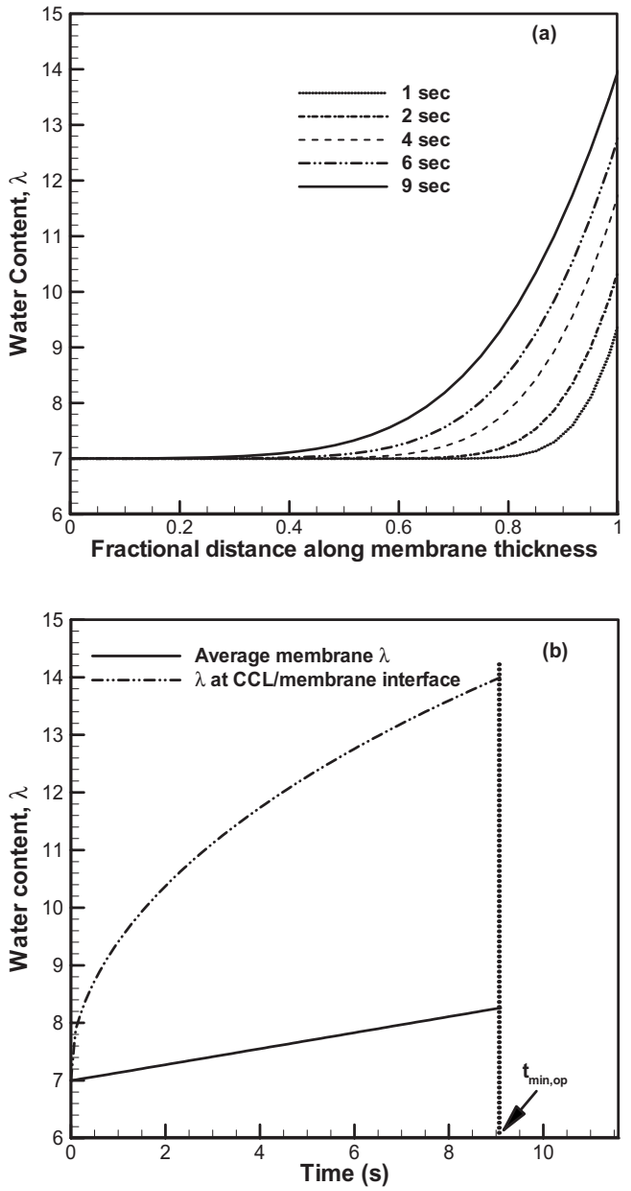

Figure 6. Water content evolution in membrane with time for infinitesimally thin CL for initial water content of 7 and start-up temperature of −20°C. (a) Water content distribution in membrane at different times and (b) average membrane water content and water content at the CCL/membrane interface vs time.

tance (calibrated to be 40 $m\Omega\ cm^2$) and using the dependence of membrane conductivity on water content given by[21]

$$\kappa_e = \exp\left[1268\left(\frac{1}{303} - \frac{1}{T}\right)\right](0.005139\lambda - 0.00326)\ \text{S/cm} \quad [19]$$

it follows that the initial water content of the membrane is approximately equal to 10 before cold start. Equation 19 is applicable for temperatures above 30°C, whereas Eq. 17 applies to the subzero temperature range. Thus, for all validation simulations, the initial water content is set at 10. Also, because the present 2 min purge leaves some residual liquid water in the CL, which can form ice/frost upon cooling, the initial ice fraction is expected to be nonzero in these experiments. In the absence of actual measurements, as a

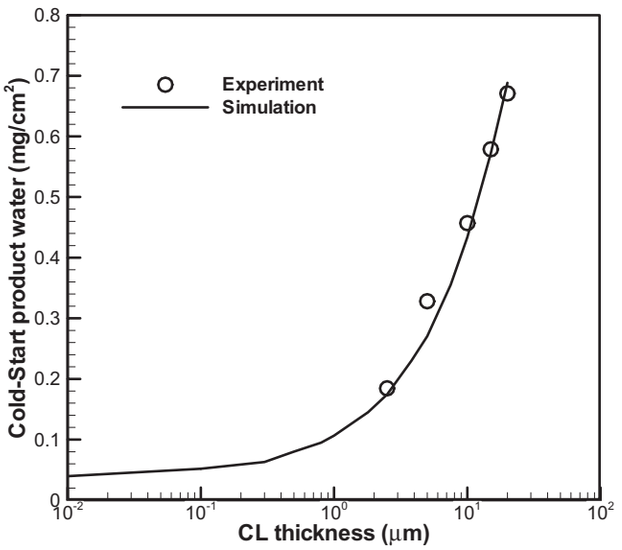

Figure 7. Experimental validation of cold-start product water from −20°C start-up temperature after 2 min gas purge with dry N_2. The initial membrane water content is estimated to be 10 H_2O/SO_3^-.

first approximation, the initial ice fraction in CCL is assumed to follow a linear increase with CL thickness given by

$$s_{ice,0} = 0.2 + 0.01(\delta_{CL} - 10) \quad [20]$$

where CL thickness, δ_{CL}, is in micrometers. The above relation could be justified by the fact that liquid water removal using short-duration purge from a thicker CL becomes more difficult, leaving a higher ice fraction initially existing in the CCL before cold start.

Figure 7 shows a comparison of the experimental data and simulation results for the cold-start product water. Simulation results agree well with experiments. This confirms the ability of the present model to capture the CL thickness effect.

Nonisothermal cold start.— While the isothermal cold-start mode provides a clear picture of the governing physics, practical PEFC operation involves rising cell/stack temperature. This section is thus concerned with the nonisothermal cold-start performance of a real PEFC and explores the corresponding effect of CL thickness. As with its isothermal counterpart, a uniform water content value of 7 is assumed initially in MEA for all simulations. All simulation cases in this section correspond to a 30 μm thick membrane as in isothermal simulations (except for the validation experiments that use Nafion 212 membranes). The current density is set to 100 mA/cm^2, and the baseline cell thermal mass is 0.4 J/cm^2 K. Two sets of simulations are performed, one at −20°C and the other at −30°C, and the results are shown in Fig. 8 and 9, respectively. For each set, eight different CL thicknesses are used (0.5, 1, 2, 4, 8, 10, 15, and 20 μm). In all the cases, an initial zero ice fraction in the CCL is assumed (same as the isothermal cold-start simulations).

Figure 8a shows temperature evolution as a function of time for eight different CL thicknesses. The total heat generation (proportional to the applied current density), the heat losses (through convective losses from bipolar plates and heat carried away by exhaust gases), and the cell thermal mass remain the same in all eight cases. Thus, all cases show the same slope of temperature evolution curves, as expected, but with varying terminating points (marked by vertical short lines in Fig. 8a). Only three cases (δ_{CL} = 10, 15, and 20 μm) exhibit a final cell temperature reaching 0°C, with the other five cases showing the terminal temperature below the freezing point, thus indicating failed start-up. It takes about 104 s for the PEFC to reach the freezing point for those three self-start cases. Thus, PEFCs with CL thicknesses of only 10 μm and above can

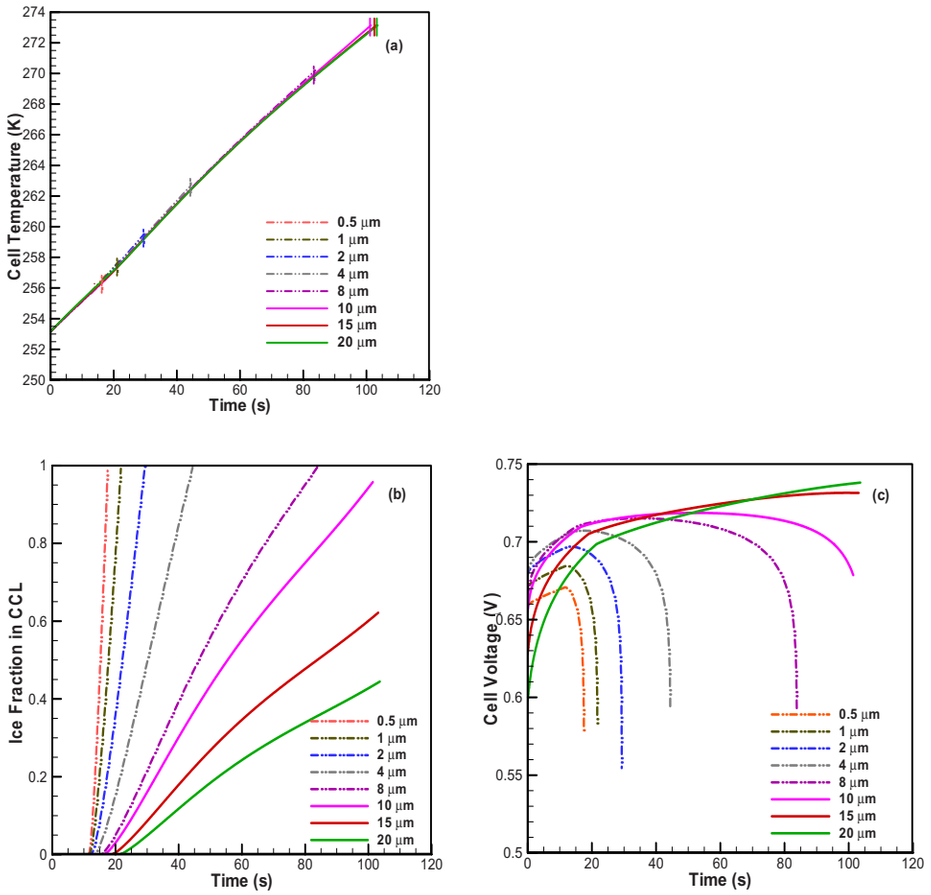

Figure 8. (Color online) Nonisothermal cold-start results for different CL thicknesses from −20°C start-up temperature (initial water content of 7). (a) Cell temperature vs time, (b) ice fraction in CCL vs time, and (c) cell voltage vs time. Note: Only cases shown by solid lines achieve successful self start-up. In the temperature plot, the end of cold start for each case is marked by a line segment. In ice fraction and voltage plots, dashed lines symbolize failed start-up cases, while solid lines stand for successful start-up cases.

achieve self-start-up under this particular operating condition. Figure 8b and c shows the corresponding ice fraction in the CCL and voltage evolution with time. Except for cases with δ_{CL} = 10, 15, and 20 μm, all other cases exhibit a final ice fraction of unity in the CCL, signifying cell shutdown. It is seen in Fig. 8b that the onset of ice formation in CL occurs slightly earlier with a thinner CL (e.g., at ~12 s for δ_{CL} = 0.5 μm compared to ~21 s for δ_{CL} = 20 μm). However, the slope of the ice fraction curves becomes much steeper with a thinner CL as this slope is inversely proportional to the CL pore volume. The latter is the main factor for short operational time or failed start-up of PEFCs with a thin CL.

The cell voltage evolution curves are shown in Fig. 8c. At the initial phase of cold start, when there is no ice precipitation in the CCL, the cell voltage experiences an increase due to temperature rise as well as membrane hydration by product water and hence a lowered ohmic voltage drop. When ice forms inside the CCL, the activation overpotential increases due to oxygen blockage and electrochemically active area reduction.[5] However, this effect becomes significant only toward the end of cold start when the ice fraction in the CCL reaches close to unity, as evidenced by the sharp drop in cell voltage (for cases with failed start-up). When the ice fraction is still low, the cell voltage shows a small increase due to improved membrane proton conductivity from water uptake and due to faster ORR kinetics with higher temperatures. The starting cell voltage (at $t = 0$) increases first with increasing δ_{CL} and then shows a large drop as δ_{CL} is made larger than 4 μm. This behavior results from two competing factors. The activation loss decreases with increasing δ_{CL}, whereas the ohmic drop due to proton transport in the electrode shows the reverse trend. When the CL thickness is smaller (below 4 μm), the former effect is predominant, but as the CL thickness is increased, the electrode ohmic drop plays a major role, causing a lower cell voltage at the start of the cold-start process.

A similar set of results for cold start from −30°C is shown in Fig. 9. Again, all the temperature curves (Fig. 9a) for various CL thicknesses show the same slope, with only one case with the largest CL thickness (δ_{CL} = 20 μm) experiencing self-start-up. Thus, for a lower start-up temperature, a thicker CL is needed for self-start-up. For the δ_{CL} = 20 μm case, it takes about 153 s to reach 0°C. The corresponding ice fraction and cell voltage curves exhibit similar trends as those of the −20°C start-up case. Ice precipitation starts at an earlier time for the −30°C cases owing to the lower water diffusivity of the membrane at the lower cell temperature and thus lower membrane water uptake. This is evident from the functional dependence of membrane water diffusivity on cell temperature and water content as follows[13]

$$D_{\text{mem}}^{H_2O} = \begin{cases} 5.93 \times 10^{-5}\lambda(e^{0.28\lambda} - 1)e^{(-4269/T)} & \text{for } 0 < \lambda \leq 3 \\ 7.97 \times 10^{-6}\lambda(1 + 161e^{-\lambda})e^{(-4269/T)} & \text{otherwise} \end{cases} \quad [21]$$

Cold start of PEFC with 1 μm thick CL.— In this section, we focus on exploring PEFC cold start with a thin CL (1 μm). With the standard set of cell parameters and material properties, the PEFC with a 1 μm thick CL cannot achieve self-start-up (Fig. 8 and 9). The goal of this section is to search for a range of cell parameters and material properties for achieving self-start-up even with a 1 μm thick CL. In particular, the effects of cell thermal mass and membrane water diffusivity are studied as important parameters affecting the cold start of PEFC with a thin CL.

Cell thermal mass, $(mC_p)_{cell}$, is a volumetric summation of heat capacities of all cell components per unit of the electrode active area. Thus, for a given heat generation and heat loss rate, a lower cell thermal mass signifies a faster temperature rise and increases the

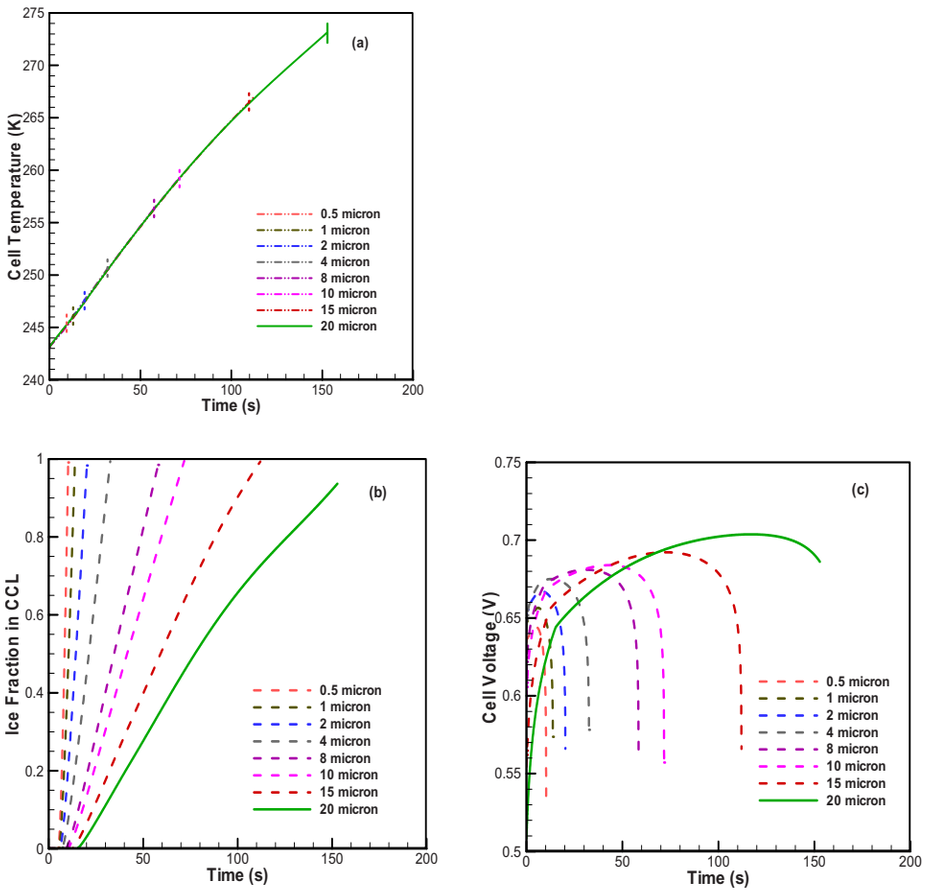

Figure 9. (Color online) Nonisothermal cold-start results for different CL thicknesses from −30°C start-up temperature (initial water content of 7). (a) Cell temperature vs time, (b) ice fraction in CCL vs time, and (c) cell voltage vs time. Note: Only cases shown by solid lines achieve successful self start-up. In the temperature plot, the end of cold start for each case is marked by a line segment. In ice fraction and voltage plots, dashed lines symbolize failed start-up cases, while solid lines stand for successful start-up cases.

chance of successful self-start-up. Three different values of cell thermal mass are studied here: the standard cell thermal mass of 0.4 J/cm^2 K, one-half (0.2 J/cm^2 K), and one-third (0.133 J/cm^2 K). For all these cases, nonisothermal cold-start simulations are performed for various start-up temperatures starting from −30°C until successful self-start-up is achieved. All other parameters are kept the same as in the nonisothermal base case. The temperature rise before cell shutdown and the corresponding cold-start product water are plotted against the start-up temperature in Fig. 10a and b, respectively. The temperature rise curves show an initial gradual increase with increasing start-up temperature followed by a rather fast increase at higher start-up temperatures. This trend results from increased membrane water uptake due to larger water diffusivity at higher cell temperatures. The trend becomes more pronounced as the cell thermal mass is reduced. For a given start-up temperature, the cell temperature increases much faster with lower cell thermal mass, and hence, it enjoys a much faster water uptake by the membrane and therefore a longer operational time before cell shutdown (and the corresponding product water and temperature rise). A PEFC can achieve self-start-up from more severe subzero conditions as the thermal mass of the cell is reduced. With a standard 0.4 J/cm^2 K cell thermal mass, a PEFC can achieve self-start-up from start-up temperatures of −10°C or above, whereas the same is true from −16 and −21°C for the 0.2 and 0.133 J/cm^2 K cases. Note a dashed–dotted straight line starting from 0°C on the x-axis of Fig. 10a and having a slope of −1. This line demarcates the "self-start-up" region from the region of "failed start-up." Such a map as displayed in Fig. 10a could be useful for selecting proper cell design parameters based on the cold-start ambient condition. The corresponding cold-start product water curves are shown in Fig. 10b as a function of start-up temperature. In Fig. 10b, there are three straight lines separating the successful from the failed start-up regions for three different values of cell thermal mass. This is because the cold-start product water representing the total heat generated must be directly proportional to the cell thermal mass for the same temperature rise ΔT needed to reach the freezing point. That is, the slope of the three straight lines displayed in Fig. 10b is directly proportional to the three values of thermal mass indicated in the figure captions. Figure 10b clearly indicates that a PEFC of 1 μm CL with 0.4 J/cm^2 K thermal mass may self-start from −10°C, but the lowest start-up temperature becomes −21°C if the cell thermal mass is lowered to 0.133 J/cm^2 K.

The membrane water diffusivity is another crucial parameter determining the cold-start capability of a PEFC. By taking up water produced during cold start, the membrane offers the PEFC more time to operate, and if the cell temperature rise is fast enough, it can reach 0°C before all CCL pores become plugged by ice. Three different membrane water diffusivities are used here for simulations of different start-up temperatures starting from −30°C until successful self-start-up is achieved. The default value of the membrane water diffusivity is shown in Eq. 21. The other two cases are 2 times and 5 times the default value. The cell thermal mass is set to the standard 0.4 J/cm^2 K. Again, all other parameters are kept the same as for other nonisothermal calculations. The results are shown in Fig. 11. In this case, both the temperature rise and the product water curves have a single linear line marking the boundary between the successful and failed start-up regions because the cell thermal mass is fixed. With increasing water diffusivity, the absorption of product water into the membrane is enhanced and so is the cold-start capability. The cell can achieve self-start-up from −10°C with the default membrane water diffusivity, while with doubled and quintupled diffusivity, successful start-up can be achieved from −13 and −14°C, respectively. Evidently, with further increase in the water diffusivity of the membrane, the cold-start capability reaches a point of dimin-

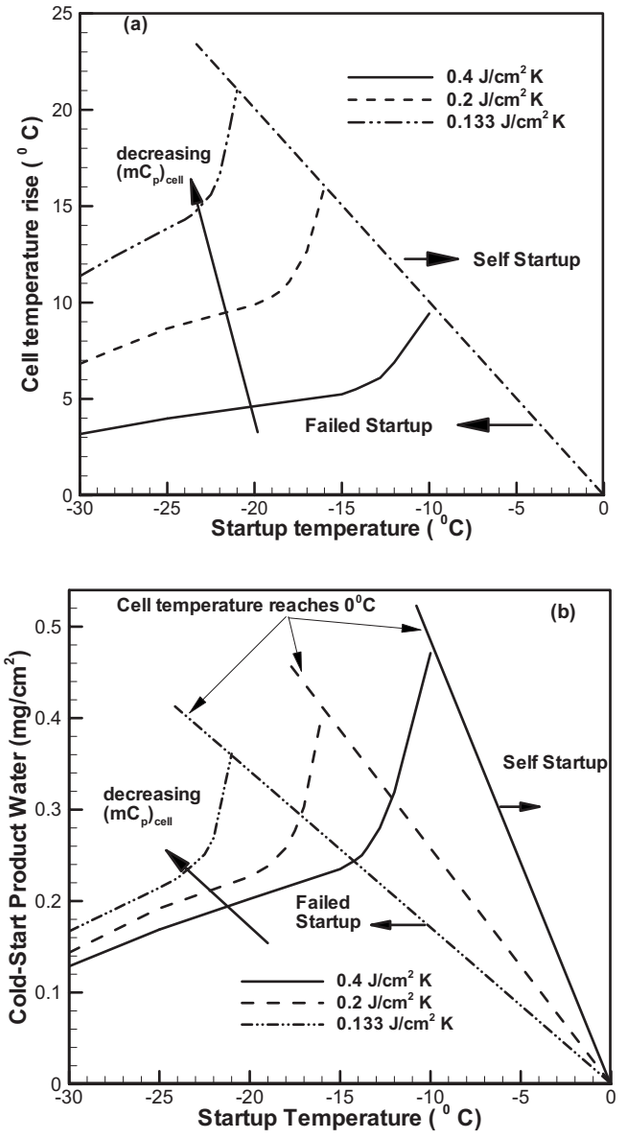

Figure 10. Effect of cell thermal mass on nonisothermal cold-start performance of a PEFC with 1 μm thick CL for varying start-up temperatures (initial water content of 7). (a) Temperature rise vs CL thickness and (b) cold-start product water vs CL thickness.

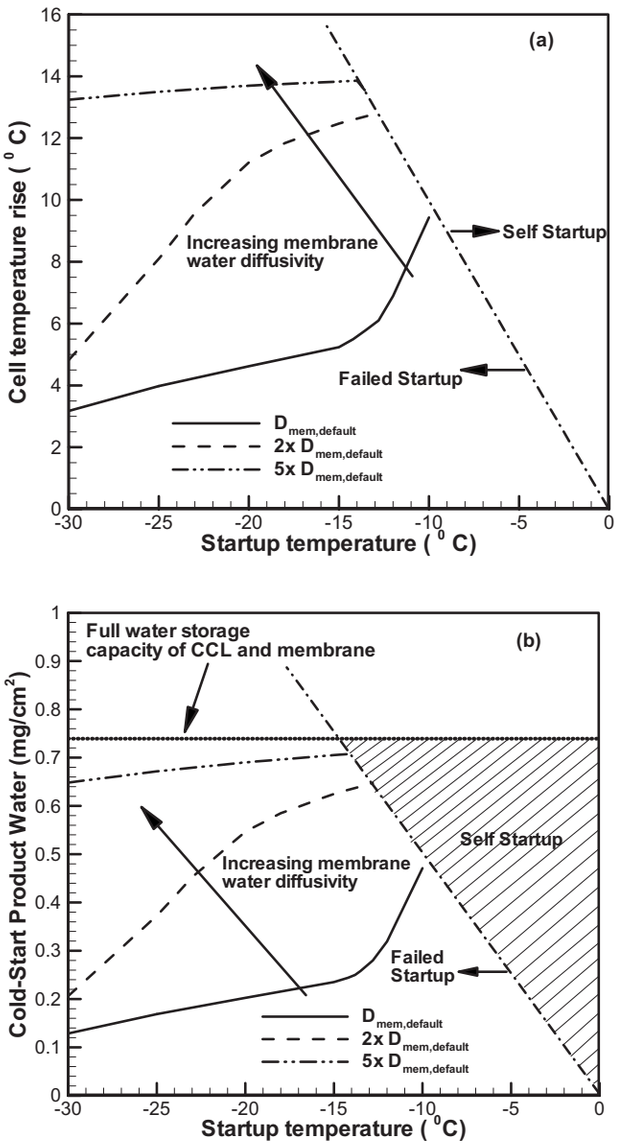

Figure 11. Effect of membrane water diffusivity on nonisothermal cold-start performance of a PEFC with 1 μm thick CL for varying start-up temperatures (initial water content of 7). (a) Temperature rise vs CL thickness and (b) cold-start product water vs CL thickness.

ishing return. The temperature rise curves for different membrane water diffusivities show different trends. With doubled diffusivity, the temperature rise increases much faster compared to the base case. This is expected as larger membrane water diffusivity signifies faster water absorption into the membrane, causing prolonged cell operation.

For the largest membrane water diffusivity, the temperature rise (and also the product water) curve shows a very high value right from the beginning (at −30°C) and remains almost flat. This could be explained by the almost full usage of the membrane water storage capacity for any start-up temperature, owing to very high membrane water diffusivity. To clarify this point further, the average membrane water content and the CCL water content evolution for the start-up temperature of −14°C are plotted against time in Fig. 12. Indeed, the average membrane water content rises to a very high value (about 13.5) at the end of the cold-start process, indicative of the full utilization of water storage throughout the membrane. The water storage capacities of the CCL ($W_{cap,CL}$) and membrane ($W_{cap,m}$) can be estimated as follows[4]

$$W_{cap,CL} = \delta_{CL}\left(\varepsilon\rho_{ice} + \varepsilon_m \frac{\rho_m}{EW}\Delta\lambda_{av,CL}M_{H_2O}\right) \quad [22]$$

$$W_{cap,m} = \delta_m \frac{\rho_m}{EW}\Delta\lambda_{av,m}M_{H_2O} \quad [23]$$

where ε is the CL porosity, ρ_{ice} is the ice density, ε_m is the volume fraction of ionomers in the CL, ρ_m and EW are the membrane density and equivalent weight, respectively, and $\Delta\lambda_{av,CL}$ and $\Delta\lambda_{av,m}$ are the differences in the average water content before and after cold start in the CL and the membrane, respectively. Using geometrical and physical parameters of the CL and membrane ($\delta_{CL} = 1$ μm, $\varepsilon = 0.5$, $\rho_{ice} = 0.918$ g/cm^3, $\varepsilon_m = 0.2$, $\delta_m = 30$ μm, and $\Delta\lambda_{av,m} = \Delta\lambda_{av,CL} = 7$), the water storage capacities are estimated to be

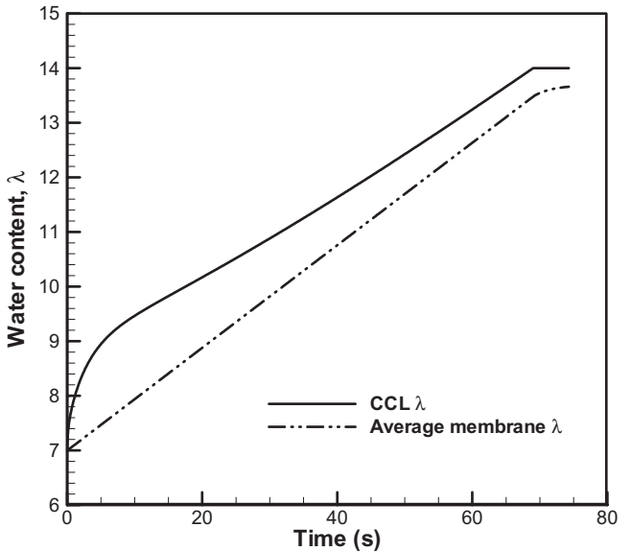

Figure 12. Water content evolution with time in CCL and membrane with −14°C start-up temperature and with highest membrane water diffusivity (5 times the default value). Note: Membrane is almost saturated (λ ~ 13.5) with water at the end of cold-start process.

$W_{cap,CL} = 0.051$ mg/cm^2 and $W_{cap,m} = 0.687$ mg/cm^2. Thus, the total water storage capacity is 0.738 mg/cm^2. This value (shown by a densely dotted line in Fig. 11b) is just slightly higher than the cold-start product water with the largest membrane water diffusivity, which again confirms the almost full utilization of the membrane water storage capacity in that case.

Figure 11b also provides a universal map to display the possible self-start-up regime, as indicated by the hatched area. This regime is bounded by the thermal mass-sloped line (to the right of it to reach the freezing point) and by the horizontal line denoting the sum of the water storage capacities in the membrane and CCL, as expressed by Eq. 22 and 23 (below the line because no cold-start product water can exceed the theoretical maximum given by it). Physically, this means that the necessary conditions for self-start-up are controlled by two factors: the water storage capacities of the membrane and CCL and cell thermal mass. To expand the self-start-up regime to the lowest temperature possible, e.g., −30°C, one has to decrease the cell thermal mass and/or increase the water storage capacities in the membrane and CCL. The latter further depends on the membrane and CL thickness as well as gas purge conditions. The shaded regime depicted in Fig. 11b represents necessary but not sufficient conditions for self-start-up.

To illustrate the utility of the map constructed in Fig. 11b, consider the necessary conditions for cold start of a PEFC with ultrathin CL from −30°C. Notice that the cell water storage capacity is essentially determined by that in the membrane in such an MEA. Then, for a membrane of 30 μm as used in Fig. 11b, the cell thermal mass must be reduced to 0.2 J/cm^2 K, as opposed to 0.4 J/cm^2 K, which intercepts at −15°C in Fig. 11b, to be able to self-start from −30°C. Alternatively, if the cell thermal mass remains at 0.4 J/cm^2 K, the membrane thickness must be increased to 60 μm. A further necessary condition for both scenarios is that the water diffusivity in the membrane must be greater than 5 times the default value expressed in Eq. 21 such that full utilization of the water storage capacity in the membrane is ensured.

One may also derive an approximate but simple formula for cold start of PEFC with a thin CL. To this end, the following approximations are invoked.

1. Water absorption in the membrane is infinitely fast so that there is full utilization of the water storage capacity in the membrane and CCL, as given by Eq. 22 and 23. This is a good approximation when the membrane water diffusivity is high and/or the start-up temperature is high.

2. Heat loss from the cell to the ambient is negligible, i.e., adiabatic start-up. This approximation is valid for cells in the middle of a stack and/or during short-duration start-up.

3. The cell voltage during cold start varies around 0.6 V. As can be seen in Fig. 8 and 9, actual cell voltage may deviate from 0.6 V by ±0.1 V, making the calculation of $(E_h - V_{cell})$ approximate by ~10%.

Under these assumptions, the heat balance condition, Eq. 16, for successful cold start is simplified to

$$(mc_p)T_o \le (E_h - V_{cell})It = \frac{2F(E_h - V_{cell})}{M_{H_2O}}(W_{cap,CL} + W_{cap,m}) \quad [24]$$

where E_h is the thermodynamic potential of the H_2/O_2 reaction ($=\Delta h/2F$ or 1.48 V) and $W_{cap,CL}$ and $W_{cap,m}$ are given by Eq. 22 and 23, respectively. Substituting relevant constants, one has

$$\frac{W_{cap,CL} + W_{cap,m}}{mc_pT_o} \ge 0.106 \text{ mg/J} \quad [25]$$

Equation 25 represents a simple criterion for the necessary conditions for self-cold start of a PEFC. The numerator denotes the water storage capacity in the MEA, the term (mc_p) in the denominator is the cell thermal mass, and T_0 represents the ambient condition. For ultrathin CL, the water storage capacity in the CL is negligible compared with that in the membrane, so Eq. 25 can further be simplified to

$$\frac{\delta_m \Delta\lambda_m}{mc_pT_o} \ge 32.7 \quad [26]$$

This formula represents a constraint among the membrane thickness (in μm), purge condition ($\Delta\lambda_m$ in H_2O/SO_3^-), cell thermal mass (in J/cm^2 K), and ambient start-up temperature (in °C) to self-start a PEFC with an ultrathin CL.

Conclusions

The effect of CL thickness or the CL pore volume on cold-start performance has been studied theoretically and experimentally, with particular focus on PEFCs having a very thin CL. The following major conclusions can be drawn.

1. The predicted cold-start product water for various CL thicknesses agrees well with corresponding isothermal cold-start experiments, demonstrating the ability of the present model to capture cold-start phenomena in PEFCs with a CL thickness ranging from 2.5 to 20 μm.

2. Under isothermal cold start, the cold-start product water decreases with decreasing CL thickness and approaches a nonzero minimum limit when the CL becomes infinitesimally thin. The minimum asymptote in the cold-start product water is linked to water absorption into the membrane and is predictable by a model problem of water transport through a membrane coated with two catalyst interfaces. This model problem could also provide an excellent experimental means to measure the transport properties of the membrane at subfreezing temperatures and under in situ cold-start conditions.

3. Nonisothermal cold-start simulations with moderately dry initial MEA ($\lambda_0 = 7$) and varying CL thicknesses show self-start-up with CL thicknesses of 10 μm and above when starting from −20°C, while self-start-up from −30°C requires a 20 μm thick CL.

4. The cell thermal mass and membrane water diffusivity affect the fate of the PEFC cold start most significantly, particularly for a thin CL. A PEFC with a 1 μm thick CL can achieve self-start-up from only −10°C (for $\lambda_0 = 7$) with standard cell thermal mass and

membrane water diffusivity. However, it can self-start from −21°C if the cell thermal mass is reduced to one-third of the standard value or from −14°C if the membrane water diffusivity is increased by a factor of 5 from the standard value (while keeping the cell thermal mass to standard value).

5. A map for the necessary conditions to ensure self-start-up has been constructed, which is bounded by the total water storage capacity in the membrane and CCL as well as cell thermal mass. Moreover, a simple interrelation between the membrane thickness, cell thermal mass, and ambient start-up temperature that represents a criterion for self-start-up of PEFC using ultrathin CL has been derived and is given in Eq. 26.

Acknowledgments

This work was supported in part by Sandia National Laboratories. Sandia is a multiprogram laboratory operated by Sandia Corporation, a Lockheed Martin Co. for the U.S. Department of Energy's National Nuclear Security Administration under contract DE-AC04-94AL85000. The ECEC team also acknowledges the support of NSF under grant no. DMS-0915153 and DOE EERE Fuel Cell Technologies Program.

Sandia National Laboratory assisted in meeting the publication costs of this article.

List of Symbols

A	electrode area, m^2
C	species concentration, mol/m^3
C_P	heat capacity, J/kg K
D	species diffusivity, m^2/s
E_h	thermodynamic potential of H_2/O_2 reaction, 1.48 V
EW	equivalent weight of dry membrane, kg/mol
F	Faraday's constant, 96,487 C/mol
h	convective heat transfer coefficient, W/m^2
h_{gs}	latent heat of vapor desublimation, J/mol
i	superficial current density, A/m^2
I	current density, A/m^2
j	transfer current density, A/m^3
K	permeability, m^2
$(mC_p)_{cell}$	cell thermal mass, J/m^2 K
$\dot{m}$	mass flow rate of gases, kg/s
M	molar mass, kg/mol
n_d	EOD coefficient, H_2O/H^+
P	pressure, Pa
$\dot{Q}$	heat generation or transfer rate per unit area, W/m^2
$\dot{q}$	water desublimation rate, mol/m^3 s
s_{ice}	ice fraction defined as the ratio of ice volume to pore volume
S	source/sink
t	time, s
Δt	time interval, s
T	temperature, K
u	superficial gas velocity, m/s
U_0	equilibrium potential, V
v	molar volume, m^3/mol
V_{cell}	cell voltage, V
W_{cap}	water storage capacity per unit area, kg/m^2

Greek

δ	thickness, m
ε	porosity or volume fraction
η	surface overpotential, V
κ	proton conductivity, S/m
λ	water content, mol H_2O/mol SO_3^-
μ	viscosity, Pa s
ξ	stoichiometric flow ratio
ρ	density, kg/m^3
σ	electronic conductivity, S/m
ϕ	phase potential, V

Subscripts

0	initial or ambient value
ϕ_e/ϕ_s	electrolyte/electron potential
a/c	anode/cathode
av	average
cap	capacity
C	species
CL	catalyst layer
gs	vapor–solid phase transition
in/out	channel inlet/outlet
m/mem	membrane
s	ice or solid phase
sat	saturated
u	momentum

Superscripts

eff	effective
i	species or component

References

1. Y. Hishinuma, T. Chikahisa, F. Kagami, and T. Ogawa, *JSME Int. J.*, **47**, 235 (2004).
2. M. Oszcipok, D. Riemann, U. Kronenwett, M. Kreideweis, and M. Zedda, *J. Power Sources*, **145**, 407 (2005).
3. L. Mao, K. Tajiri, S. Ge, X. G. Yang, and C. Y. Wang, Abstract 998, The Electrochemical Society Meeting Abstracts, Vol. 502, Los Angeles, CA, Oct 16–21, 2005.
4. S. Ge and C. Y. Wang, *Electrochem. Solid-State Lett.*, **9**, A499 (2006).
5. L. Mao and C. Y. Wang, *J. Electrochem. Soc.*, **154**, B139 (2007).
6. K. Tajiri, Y. Tabuchi, and C. Y. Wang, *J. Electrochem. Soc.*, **154**, B147 (2007).
7. L. Mao, C. Y. Wang, and Y. Tabuchi, *J. Electrochem. Soc.*, **154**, B341 (2007).
8. K. Tajiri, Y. Tabuchi, F. Kagami, S. Takahashi, K. Yoshizawa, and C. Y. Wang, *J. Power Sources*, **165**, 279 (2007).
9. S. Ge and C. Y. Wang, *Electrochim. Acta*, **52**, 4825 (2007).
10. J. Hou, H. Yu, B. Yi, Y. Xiao, H. Wang, S. Sun, and P. Ming, *Electrochem. Solid-State Lett.*, **10**, B11 (2007).
11. E. L. Thompson, J. Jorne, and H. A. Gasteiger, *J. Electrochem. Soc.*, **154**, B783 (2007).
12. S. Ge and C. Y. Wang, *J. Electrochem. Soc.*, **154**, B1399 (2007).
13. F. Jiang, W. Fang, and C. Y. Wang, *Electrochim. Acta*, **53**, 610 (2007).
14. J. Li, S. Lee, and J. Roberts, *Electrochim. Acta*, **53**, 5391 (2008).
15. E. L. Thompson, J. Jorne, W. B. Gu, and H. A. Gasteiger, *J. Electrochem. Soc.*, **155**, B625 (2008).
16. E. L. Thompson, J. Jorne, W. B. Gu, and H. A. Gasteiger, *J. Electrochem. Soc.*, **155**, B887 (2008).
17. F. Jiang and C. Y. Wang, *J. Electrochem. Soc.*, **155**, B743 (2008).
18. K. G. Gallagher, B. S. Pivovar, and T. F. Fuller, *J. Electrochem. Soc.*, **156**, B330 (2009).
19. F. Jiang, C. Y. Wang, and K. S. Chen, *J. Electrochem. Soc.*, **157**, B342 (2010).
20. C. Y. Wang, X. G. Yang, Y. Tabuchi, and F. Kagami, in *Handbook of Fuel Cells*, Vol. 6, W. Vielstich, H. Yokokawa, and H. A. Gasteiger, Editors, Chap. 59, John Wiley & Sons, New York (2009).
21. T. E. Springer, T. A. Zawodinski, and S. Gottesfeld, *J. Electrochem. Soc.*, **138**, 2334 (1991).
22. K. Tajiri, C. Y. Wang, and Y. Tabuchi, *Electrochim. Acta*, **53**, 6337 (2008).